Quantum spin-liquid states in an organic magnetic layer and molecular rotor hybrid

Péter Szirmai[a], Cécile Mézière[b], Guillaume Bastien[c], Pawel Wzietek[d], Patrick Batail[b], Edoardo Martino[a], Konstantins Mantulnikovs[a], Andrea Pisoni[a], Kira Riedl[e], Stephen Cottrell[f], Christopher Baines[g], László Forró[a,1], and Bálint Náfrádi[a,1]

[a]Laboratory of Physics of Complex Matter, Ecole Polytechnique Fédérale de Lausanne, CH-1015 Lausanne, Switzerland, 1015; [b]Laboratoire MOLTECH-Anjou, CNRS and Université d'Angers, 49045 Angers, France, 49045 Angers; [c]Institute of Organic Chemistry and Biochemistry, Academy of Science of the Czech Republic, 166 10 Prague 6, Czech Republic; [d]Laboratoire de Physique des Solides, CNRS and Université de Paris-Sud, 91405 Orsay, France, 91405; [e]Institut fur Theoretische Physik, Goethe-Universitat Frankfurt, 60438 Frankfurt am Main, Germany; [f]ISIS Muon Group, Science and Technology Facilities Council (STFC), Didcot OX11 0QX, United Kingdom; and [g]Laboratory for Muon Spin Spectroscopy, Paul Scherrer Institute, 5232 Villigen, Switzerland

Edited by Stuart Brown, University of California, Los Angeles, CA, and accepted by Editorial Board Member Zachary Fisk September 30, 2020 (received for review January 6, 2020)

The exotic properties of quantum spin liquids (QSLs) have continually been of interest since Anderson's 1973 ground-breaking idea. Geometrical frustration, quantum fluctuations, and low dimensionality are the most often evoked material's characteristics that favor the long-range fluctuating spin state without freezing into an ordered magnet or a spin glass at low temperatures. Among the few known QSL candidates, organic crystals have the advantage of having rich chemistry capable of finely tuning their microscopic parameters. Here, we demonstrate the emergence of a QSL state in [EDT-TTF-CONH$_2$]$_2^+$[BABCO$^-$] (EDT-BCO), where the EDT molecules with spin-1/2 on a triangular lattice form layers which are separated by a sublattice of BCO molecular rotors. By several magnetic measurements, we show that the subtle random potential of frozen BCO Brownian rotors suppresses magnetic order down to the lowest temperatures. Our study identifies the relevance of disorder in the stabilization of QSLs.

quantum spin liquid | QSL | molecular rotor | triangular lattice | quenched randomness

Localized spins in magnetically interacting spin systems are generally expected to order at low temperatures. In some cases, geometrical frustration (1–6) may suppress conventional magnetic ordering, and a unique, fluctuating, quantum-disordered state emerges (7, 8). This macroscopic collective state, the so-called quantum spin liquid (QSL) (9, 10), may be, for example, distinguished by its exotic spin excitations with fractional quantum numbers (7, 11).

In one-dimensional spin systems, quantum fluctuations arise naturally. In dimensions greater than one, organic materials were among the first examples of QSL candidates (1–3). These systems either have nearly isotropic triangular lattices like frustrated magnetic structures, e.g., κ-(ET)$_2X_2$ (CN)$_3$ (X = Cu, Ag) (1, 12) and β-EtMe$_3$SbPd[(dmit)$_2$]$_2$ (2), or have been approximated by the quasi–one-dimensional limit, as exemplified by κ-(ET)$_2$B(CN)$_4$ (13) and κ-H$_3$ (Cat-EDT-TTF)$_2$ (4). A gapless or weakly gapped QSL state develops in all these compounds, independent of the level of frustration (14, 15).

Despite recent progress, the investigation of QSL states is still a major experimental and theoretical challenge (9, 14, 16, 17). Notably, the geometrical frustration of the spin-1/2 isotropic equilateral triangular lattice in the nearest-neighbor Heisenberg model is insufficient to induce a QSL phase, since the ground state is a three-sublattice Néel order (18–20). To promote the emergence of a QSL phase, different extensions were considered in theoretical models, such as higher-order terms (21), e.g., the four-spin ring-exchange interaction, or further-neighbor interactions (22).

Organic crystals always have a minute amount of defects (23), but their importance in theoretical studies was omitted for a long time. Only a few works studied the interplay of magnetic frustration and quenched bond randomness to induce or support a QSL state (23–25). It came as a surprise that the X-ray irradiation of the weakly frustrated, long-range ordered antiferromagnet, κ-(ET)$_2$Cu[N(CN)$_2$]Cl was reported to lead to the stabilization of a disorder-driven QSL state (26). To understand systematically the role of quenched randomness in two-dimensional (2D) materials, methods are needed to introduce it in organic systems without seriously damaging the underlying structure. In such materials, weakly randomized spin–spin interactions may lead to the emergence of low-temperature magnetic ground states by altering the effect of the spatial anisotropy of exchange couplings (23, 25, 26).

We here report a highly original QSL system, [EDT-TTF-CONH$_2$]$_2^+$ [BABCO$^-$] (abbreviated EDT-BCO) (Fig. 1). In the EDT layers (27), triangularly organized dimers carry a spin-1/2 magnetic moment. These are separated by a sublattice of carboxylate anions centered by a chiral bicyclo[2.2.2]octane (BCO), called rotors, having conformational and rotational degrees of freedom (Fig. 1 *B* and *C* and *SI Appendix*, Fig. S1) (27). The spin Hamiltonian of the EDT layer alone predicts either a spiral or a collinear magnetic order (28, 29). We have explored the material

Significance

A better understanding of quantum spin liquids (QSLs), where spin dimer configurations are fluctuating even at the lowest temperatures, could be of use in quantum information, in superconducting or other technologies. This macroscopic collective state typically arises from geometrical frustration or low dimensionality. In the layered EDT-BCO, we report a QSL state, which is generated, on different bases, with the intrinsic disorder. The spins in the EDT plane despite a weak frustration would magnetically order but the disorder potential coming from the molecular rotors in the BCO plane prevents it. With multiple experimental probes, the stabilization of a QSL state is demonstrated with signatures of orphan spins, as defects between the QSL domains.

Author contributions: P.Sz., L.F., and B.N. designed research; P.Sz., P.W., E.M., K.M., A.P., K.R., S.C., C.B., L.F., and B.N. performed research; C.M., G.B., and P.B. synthesized molecules/crystals; P.Sz., P.W., P.B., E.M., K.M., A.P., K.R., S.C., C.B., L.F., and B.N. analyzed data; and P.Sz., C.M., G.B., P.W., P.B., E.M., K.M., A.P., K.R., S.C., C.B., L.F., and B.N. wrote the paper.

The authors declare no competing interest.

This article is a PNAS Direct Submission. S.B. is a guest editor invited by the Editorial Board.

[1]To whom correspondence may be addressed. Email: laszlo.forro@epfl.ch or nafradi@yahoo.com.

This article contains supporting information online at https://www.pnas.org/lookup/suppl/doi:10.1073/pnas.2000188117/-/DCSupplemental.

First published November 5, 2020.

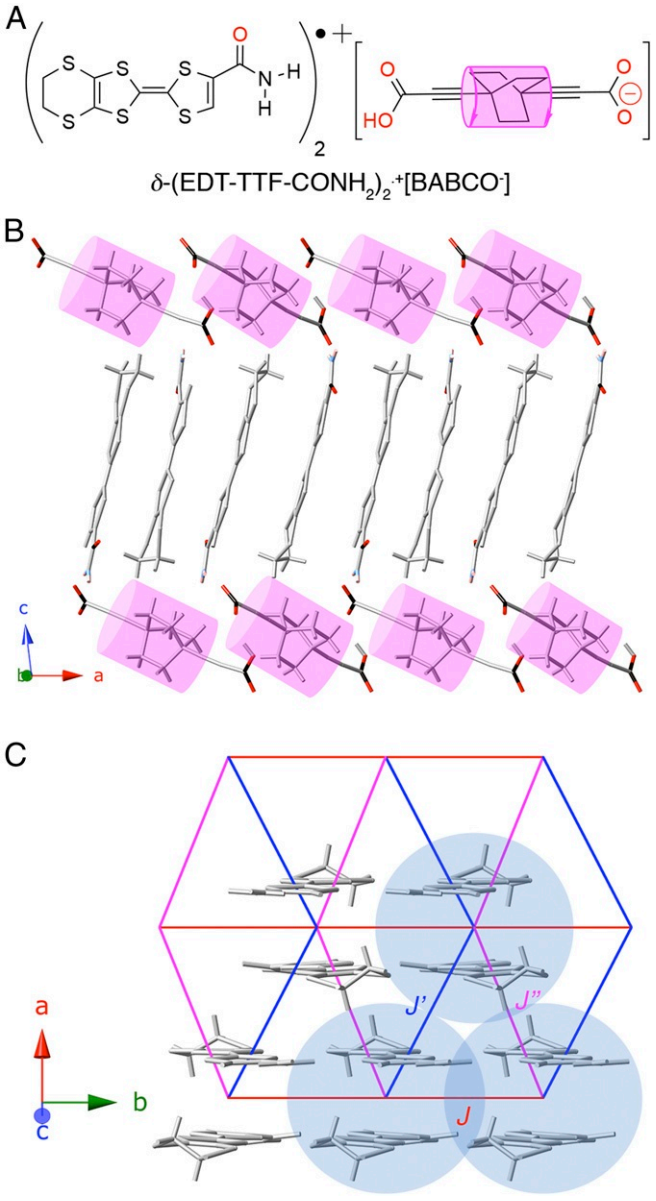

Fig. 1. $[EDT\text{-}TTF\text{-}CONH_2]_2^+[BABCO^-]$: a crystalline hybrid of molecular conductor and molecular rotor (27). (*A*) The two molecular units in $[EDT\text{-}TTF\text{-}CONH_2]_2^+[BABCO^-]$. The pink cylinder illustrates the rotational degree of freedom of BCO fragments around the rod axle. An additional, torsional degree of freedom drives $\lambda \leftrightarrow \delta$ conformational mutations of chiral BCO rotators in the lattice (31), as illustrated in *SI Appendix*, Fig. S1. (*B*) Layers of $[EDT\text{-}TTF\text{-}CONH_2]_2^+$ radical cations alternate with an array of rotators in dynamic equilibrium in the lattice. (*C*) The topology of the distorted triangular lattice of mixed-valence dimers defined by exchanged interactions $J : J' : J'' = 314{:}172{:}105$ K.

with magnetic resonance techniques at various timescales—proton nuclear magnetic resonance (^{1}H-NMR), electron spin resonance (ESR), and down to 20 mK muon spin rotation (μSR)—and have found no sign of emerging long-range magnetic order, but rather a QSL state. In our interpretation, the EDT layer's magnetic order is broken by the disorder potential coming from the rotationally frozen BCO molecules at low temperatures. Furthermore, its conformational changes (*SI Appendix*, Fig. S1) have a low activation energy (<50 K) (30), and the tunneling between two conformations (denoted as λ and δ) happens even at very low temperature, exerting an additional source of disorder (27, 30, 31). The attractive spinoff of our study is the notion that the nature and change of dynamics of functional rotors in the anionic layer could provide a tunable tool toward designing additional QSL materials.

Results

In density functional theory (DFT) calculations, we determined the exchange couplings of a hypothetical, disorder-free parent system of EDT-BCO, where the BCO units are placed uniformly (*Materials and Methods* and *SI Appendix*, Table S1). They give a distorted triangular lattice of dimers with nearest-neighbor overlap integrals and antiferromagnetic exchanges of $t : t' : t'' = 1.00 : 0.75 : 0.60$ ($J : J' : J'' = 314 : 172 : 105$ K) in between the molecular EDT dimers (Fig. 1*C*). This strong spatial anisotropy in J places our material in between the frustrated, near-equilateral triangular lattice and the quasi–one-dimensional limit. According to previous theoretical works (32, 33), this weak frustration does not support a QSL ground state. Rather, chiral or collinear magnetic-ordered phases are expected in EDT-BCO.

In strong contrast to these theoretical predictions, all our experiments—ESR, NMR, and μSR measurements—suggest the absence of long-range magnetic order and the emergence of a QSL. We now first discuss the results of the ESR experiments.

From the resonance line, one can deduce the electronic spin susceptibility (χ) and the spin relaxation rate through the linewidth ΔB_{pp} and, from its position, the g factor. All three quantities can detect magnetic ordering or even fluctuations. These measurements were performed in an outstandingly broad frequency range from 4 to 420 GHz, corresponding to magnetic fields from 0 to 16 T, giving a rarely seen resolution in interactions.

ESR, unlike static measurements, can deconvolute the contribution of different spin systems having distinct g factors. For example, this allows the separation of the bulk magnetism from possible Curie impurity contributions. Above 50 K, χ is almost constant (Fig. 2*A*), like that of strongly antiferromagnetically interacting systems, thus confirming our DFT calculations.

The value of the spin susceptibility is close to those observed for other organic spin-liquid candidates (κ-$(ET)_2X_2(CN)_3$ (X = Cu, Ag)) (1, 12). It was suggested to be proportional to the spinon density of states and to scale inversely with the spinon hopping amplitude governed by a strong exchange coupling in the range of $J/k_B = 300$ to 350 K. However, χ in EDT-BCO does not decrease at low temperatures, unlike in disorder-free anisotropic triangular lattice models (29). Instead, we observe a weak upturn below ~50 K. In principle, it could be a sign of Curie impurities or the emergence of a magnetic order. Our experiments, however, suggest a different origin. The upturn of χ does not show sample-to-sample variation, as would be the case for impurities. In *SI Appendix*, Fig. S2, χ of different batches of EDT-BCO are shown, which all follow a common, $\chi \propto T^{-0.4}$ power-law increase at low temperatures. Thus, it is an intrinsic characteristic of the EDT-BCO material, not an impurity signal. We come back to this interpretation in *Discussion*.

Precise measurements of the g factor by changing temperature or magnetic field could detect the development of internal magnetic fields or any additional contribution to spin anisotropies. Experimentally, the g factor remains unchanged within our precision in temperature (Fig. 2 *A*, *Inset*) and up to the highest frequencies (largest magnetic fields; *SI Appendix*, Fig. S3). This demonstrates the absence of an emerging magnetic order or a static magnetization.

The ESR linewidth, ΔB_{pp}, at temperatures above 30 to 40 K with its maximum around 70 K, is characteristic of other

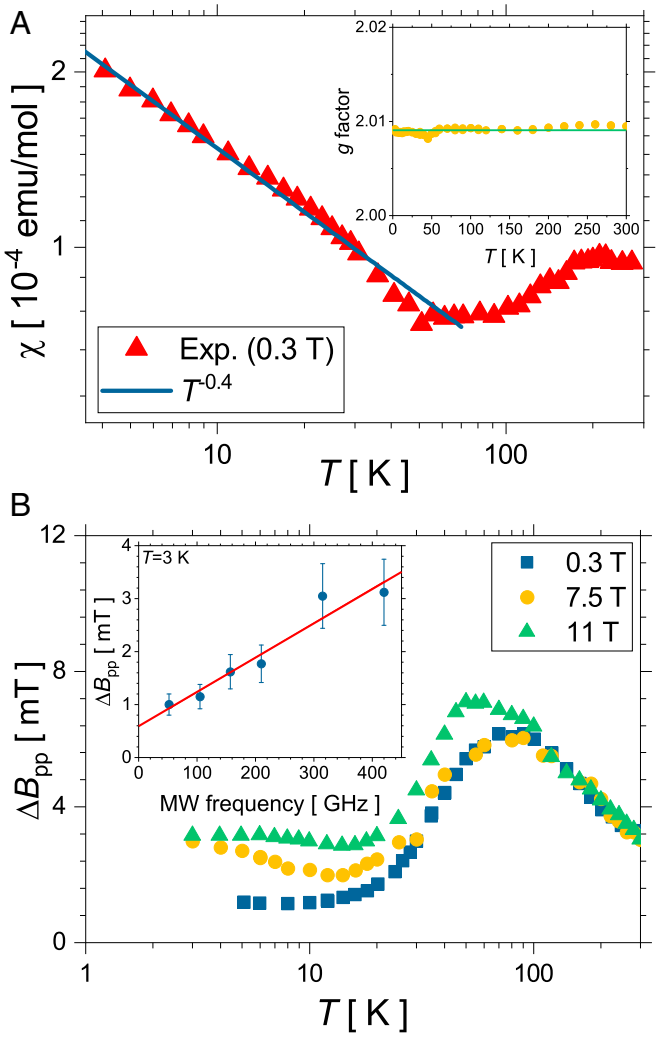

Fig. 2. (*A*) Spin susceptibility of EDT-BCO measured by ESR shown on a logarithmic plot with a power-law dependence at low temperatures (*SI Appendix*, Fig. S2). *Inset* shows the *g* factor in the whole temperature range. (*B*) Field dependence of the ESR linewidth, ΔB_{pp}. *Inset* shows its frequency dependence for $B \parallel c$ direction. The solid line is a fit.

materials within the same family, such as κ-$(ET)_2Cu_2(CN)_3$ (34). For the interpretation of this temperature range, we refer to ref. 34. Our report focuses on the low-temperature portion, where we could find signatures of QSL behavior.

Even if no static magnetization develops, a low-temperature short-range fluctuating magnetic order may arise in the presence of high magnetic fields in the proximity of an ordered state. These would lead to a critical broadening of the ESR linewidth, ΔB_{pp} (35). For example, the Dzyaloshinskii–Moriya interaction—which is present in EDT-BCO—was evoked in organic spin liquids, to induce weak antiferromagnetic order at high magnetic fields and low temperatures (36). The Bose–Einstein condensation of spinon excitations may also occur (15). Field-induced effects due to magnetic anisotropies would emerge as a nonlinear, minimally quadratic field dependence and at least an order of magnitude increase at low temperatures in ΔB_{pp}. Such a critical behavior was observed earlier, e.g., in κ-$(ET)_2Cu[N(CN)_2]Cl$ (37, 38). In our samples, ΔB_{pp} has a weak temperature dependence below 10 K. What is also significant is that it does not increase nonlinearly as a function of the magnetic field at fixed temperatures (Fig. 2 *B*, *Inset*). This demonstrates the absence of critical magnetic fluctuations toward an ordered state of up to 15 T. Nevertheless, the ESR linewidth does change linearly with magnetic fields, in contrast to a noninteracting paramagnet. This illustrates that fast spin fluctuations are present at low temperatures. As in a motional narrowing-like effect, approaching the frequency of spin fluctuations would lead to a peak and a substantial broadening of ΔB_{pp} (39, 40).

NMR measurements could bring information both about dynamical changes in the structure, and about magnetic interactions at timescales much longer than that of ESR. First, NMR measurements of ^1H can give insight into the emerging disorder potential coming from the BCO rotors by investigating its rotational degrees of freedom (Fig. 1*A*). The BCO units are typically fast Brownian rotators, with one to hundreds of gigahertz rotation at room temperature, depending on their surroundings (ref. 41 and references therein). Based on the energy barriers of the most significant, barrier-determining C–H–O hydrogen bond interactions, the rotation is expected to have larger frequencies.

However, previous ^1H-NMR investigations have shown that the motion of the BCO rotators in EDT-BCO is much slower than in other structures (27), presumably due to the stronger EDT and BCO interactions.

Fig. 3*A* shows that the NMR spin-lattice relaxation is dominated by the rotor motion above 70 K, resulting in a significant dynamic. The peak at 270 K comes from the matching of the rotational frequency with the NMR probing frequency (62 MHz). On cooling down, as it could be read from T_1^{-1}, rotors slow down with an activation energy of $E_a/k_B \approx$ 2,000 to 2,500 K and an attempt frequency (inverse correlation time) of $A = 1/\tau_c = 3$ to $4 \cdot 10^{12}$ s^{-1} (27), fitted using the Bloembergen–Purcell–Pound (BPP) theory (42).

Therefore, the rotational degree of freedom becomes severely impeded below ~100 K, with the rotor blades stopping randomly at any of three equilibrium positions (27). The upturn of T_1^{-1} below 15 K has another origin from that of the freezing of the BCO rotation, and it corroborates with the upturn in the second moment, shown in Fig. 3*B* in the same temperature range and explained below.

Low-lying electronic spin excitations influence the NMR relaxation at low temperatures, so T_1^{-1} could be a sensitive gauge to detect frozen static magnetic moments, as well. Fig. 3 *A*, *Inset* shows representative NMR spectra below 70 K. They are typical of nuclear dipolar fields and there is no significant broadening down to 5 K, the lowest temperatures studied. Nevertheless, in Fig. 3*B*—where the second moment, $\sqrt{<f^{2nd}>}$, of ^1H-NMR spectra is plotted (deduced from the linewidth)—a weak increase is noticed emerging from short-range magnetic correlations below 15 K (1). Note that above 70 K, $\sqrt{<f^{2nd}>}$ is also dominated by the BCO rotation. However, this weak increase cannot stem from ordered magnetic moments, as its value would be well below 0.01 μ_B above 5 K. It is rather the signature of a magnetically disordered, QSL behavior.

We believe that the weak increase in T_1^{-1} in Fig. 3*A* below 10 K has the same origin, that is, of critical magnetic fluctuations. Its functional dependence seems to support an unusual power law of $T_1^{-1} \propto T^{-\alpha}$ with $\alpha = 0.8(2)$.

The crucial experiment to confirm the absence of local freezing of magnetic moments, and to support the QSL state, is the zero-field μSR, measured down to 20 mK. Since muon has a magnetic moment, and it is implanted in the material as a local probe, it is an especially sensitive tool for probing local magnetic fields.

The depolarization curves of such measurements (*SI Appendix*, Fig. S6) show coexisting random static fields associated with, for example, the dipolar coupling of the muon and quasi-static nuclear moments and dynamically fluctuating fields associated with electronic spin fluctuations. To extract the relaxation rate of this last parameter, one has to fit the asymmetry function as

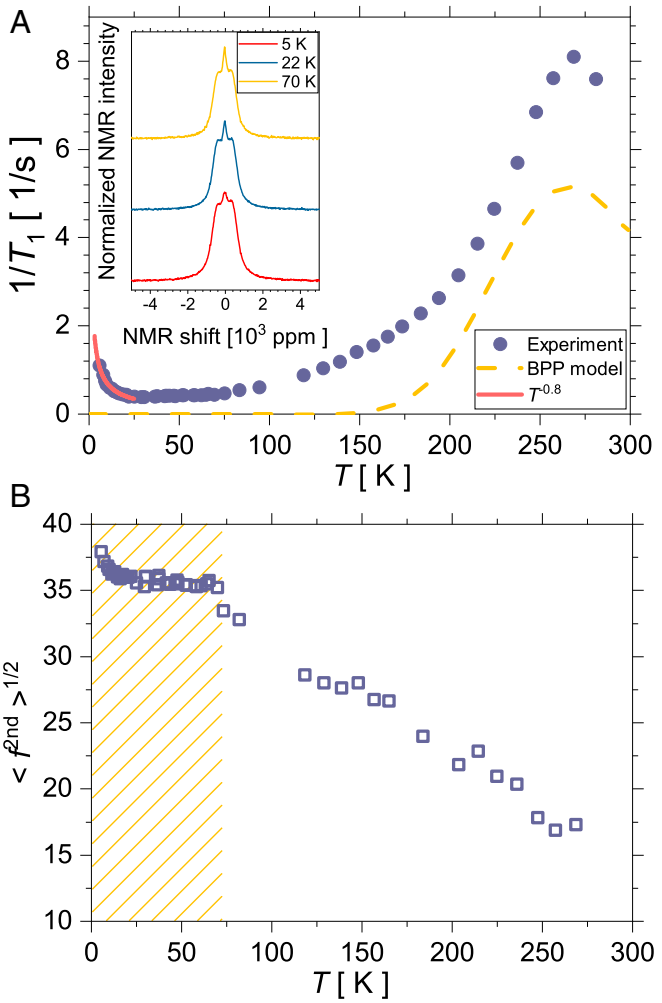

Fig. 3. (*A*) Single-component ^{1}H-NMR spin-lattice relaxation rate as a function of temperature (solid circles) and simulation of the motion-induced component (dashed line). Power-law fit is shown as an eye guide to low-temperature upturn of $T_1^{-1} \propto T^{-0.8}$. (*Inset*) NMR spectra at three characteristic temperatures measured at 62 MHz (2 T). (*B*) The second moment of ^{1}H-NMR spectra deduced from the linewidths. Below 70 K, the motion of the rotors is completely stopped, and a slow increase is observed, indicating the development of antiferromagnetic correlations.

$A(t) - A_0 = G_{KT}(\Delta, t) \cdot e^{-\lambda t}$ (43). Here, G_{KT} is the static zero-field Kubo–Toyabe function describing spatially random fields with many different frequencies overlapping, Δ is the distribution width of the depolarization rate of the static nuclear spin contributions, and λ describes the relaxation rate of electronic spin fluctuations. To identify critical properties in our magnetically fluctuating system, we calculate the electron spin fluctuation rate of μSR spectra, $\Gamma(T) = 1/\lambda(T)$ (following ref. 15).

As seen in Fig. 4*A*, $\Gamma(T)$ (normalized to its value at 5 K) exhibits only slow changes in temperature without a critical slowing down of the electronic spin fluctuations. That is, it shows a substantial decrease in $\Gamma(T)$, which would be the sign of magnetic ordering. The persistent fluctuations, and the constant $\Gamma(T)$ below 0.5 K, suggest a spin-fluctuating QSL state down to 20 mK. This constant low-temperature spin relaxation, of central importance for our study, is a universal characteristic of several spin-liquid candidates (6, 15, 44, 45). The overall shape of $\Gamma(T)$ resembles that of κ-$(ET)_2Cu_2(CN)_3$, the canonical QSL material, extensively studied by Pratt et al. (15). In their analysis, they have attributed to the various regimes (Fig. 4 *A*, hatched regions) different quantum critical behaviors, except that above 100 K, where $k_B T$ reaches the characteristic exchange coupling strength. For a detailed discussion of these regimes, we refer to their work. It should be noted that $\Gamma(T)$ in both materials presents a relatively weak temperature dependence over the whole temperature range. This reveals the absence of a substantial slowing down of spin dynamics in these organic QSL candidate systems.

We focus our attention to the range below 0.5 K where the signature of QSL is measured. To identify the dynamics of the spin fluctuations in a QSL, one needs to perform longitudinal field dependence measurements of μ^+ relaxation (λ_{LF}; *SI Appendix*, Figs. S6–S8).

On general grounds, the field dependence of λ_{LF} can be attributed to the specific decay of the electronic spin dynamical autocorrelation function, defined as $S(t) = \langle \mathbf{S}(t)\mathbf{S}(0) \rangle$, with $\lambda_{LF} \approx 2\delta^2 \int_0^\infty S(t)\cos(\omega_L t)\,dt$, where δ is the width of the distribution of fields experienced by the muon for different electronic spin configurations, and ω_L is the muon Larmor frequency.

We plot λ_{LF} at 80 mK in Fig. 4*B*. Its field dependence roughly is $\lambda_{LF} \propto B^{-0.6}$. A power-law behavior ($\lambda_{LF} \propto B^{-n}$) of the

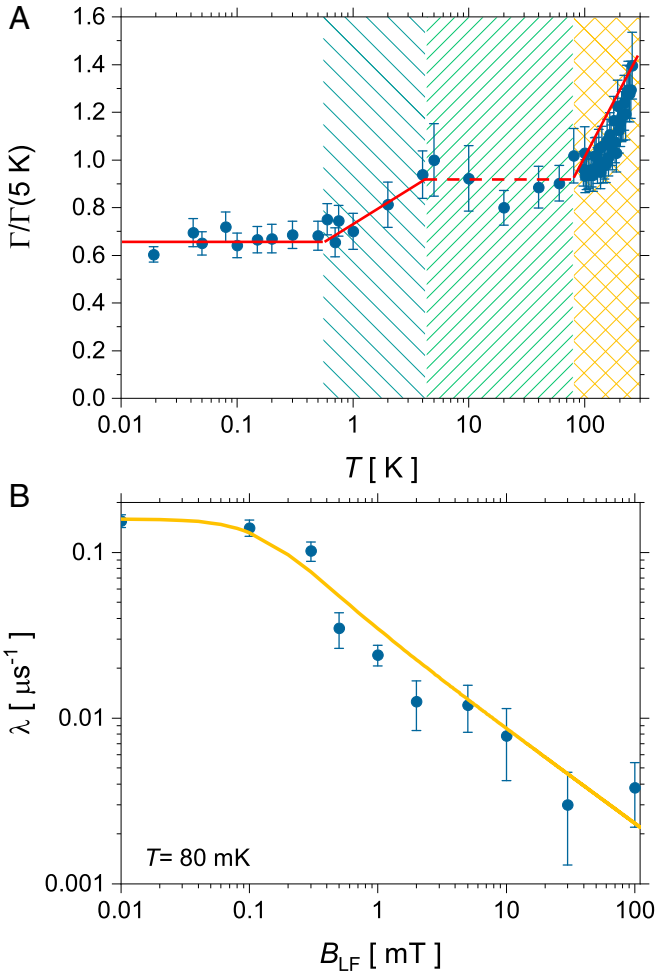

Fig. 4. (*A*) Zero-field μSR spin fluctuation rate (normalized to 5 K) shows a weak temperature dependence. Red eye guides and hatched areas highlight the proposed relaxation regimes. Below 0.5 K, the constant spin fluctuations indicate persistent spin dynamics. (*B*) Longitudinal field-dependent μSR relaxation at $T = 80$ mK. The solid line is a fit to the field dependence, characterizing 2D spin excitations with power-law spin–spin correlations. We note that the point shown at 0.01 mT corresponds to the zero-field μSR experiment.

longitudinal field dependence has been evoked in one-dimensional antiferromagnetic spin chains (46), and in disordered systems, including quantum spin liquids. Nevertheless, the observed power-law exponent of $n \approx 0.6$ deviates substantially from the one-dimensional case of $n \leq 0.5$, observed experimentally and calculated (46–48) (*SI Appendix*).

For spin-disordered systems, the decay of the average autocorrelation function is often dominated by rare regions that exhibit long autocorrelation times, and it can be described by $S(t) \sim t^{-x} e^{-\nu t}$, where the exponent x measures the effective disorder strength, and the exponential part gives the long time cutoff (49–52). To extract x, we have obtained a general functional form of μ^+ relaxation rate as

$$\lambda_{\mathrm{LF}} \propto \cos\left[(x-1)\tan^{-1}\left(\frac{\omega_{\mathrm{L}}}{\nu}\right)\right]\left(\frac{1}{\omega_{\mathrm{L}}^2+\nu^2}\right)^{(1-x)/2} \quad [1]$$

which corresponds to $\lambda_{\mathrm{LF}} \propto B^{x-1}$ in the limit $\omega_{\mathrm{L}} \gg \nu$. On the basis of experimental and numerical results for random spin systems (49, 50), it is expected that $x < 0.8$.

Indeed, we observed that the behavior of EDT-BCO is consistent with $x \approx 0.4$ (*SI Appendix*, Fig. S8). Similar longitudinal field dependence was found at all temperature points below 1 K. The best fit for 80 mK corresponds to the yellow curve in Fig. 4*B*. The value of x is consistent with the range observed for other spin-liquid candidates, where disorder is thought to play a prominent role, including the inorganic triangular lattice spin-liquid candidate $YbMgGaO_4$ ($x \approx 0.66$) (53) and the kagome antiferromagnet, $MgCu_3(OH)_6Cl_2$ ($x \approx 0.33$) (45).

Discussion

The DFT calculation for the EDT sublattice gives a strong anisotropy in the exchange energies on the triangles composed of EDT molecules. With distinct values of J, the system is far from being frustrated, like on an equilateral triangle, but it is not anisotropic enough to be considered strictly one-dimensional. All facts taken seriously, this would impose a long-range magnetic order. But none of the experimental methods applied—ESR, NMR, and μSR—detect a magnetic order in our high-quality crystals.

The circumstance which could explain this mismatch between DFT and experiments is the disorder which is generated by the frozen-in position of the BCO rotors at low temperatures. This disorder can affect the foreseen magnetic ordering in the EDT planes in two ways: first, by decoupling the planes, rendering them strongly 2D. And in the spirit of the Mermin–Wagner theorem, there should not be a long-range order in 2D. The second way is via the randomized rotor configurations provoking disorder at nearly every unit cell. Then almost every exchange interaction is affected, and the coherent couplings of the magnetic moments in the plane are precluded. Nevertheless, the finite crystal size and anisotropies which are usually present in real samples are circumstances that could release the restrictions of the Mermin–Wagner theorem. We believe that the second scenario, the disorder coming from the BCO molecules, is responsible for the absence of the magnetically ordered state in EDT-BCO.

DFT calculations would be important to confirm our statement that the disorder potential of the rotors precludes the long-range magnetic order. However, the effect of disorder needs to consider a reasonably large number of unit cells. The magnetic coupling constants without disorder could be obtained straightforwardly, although the layers of rotors have not been taken explicitly into account, but already the unit cell contains 160 atoms. When dealing with the effect of disorder originating from the rotor layers, the required effective unit cell would be too large to study. Furthermore, to resolve energy differences between various magnetic configurations of the order of 100 to 200 K (≈10 meV), one would need a very high precision calculation given the large number of atoms in the supercell. Computation-wise, this is an extremely hard task, and it is reserved for future studies.

The QSL state does not mean that there cannot be fluctuating, short-range magnetic interactions, as ESR and NMR measurements indicate through the sample-independent $\chi \propto T^{-0.4}$ spin susceptibility and the low-temperature upturn in T_1^{-1} and NMR linewidth. In our interpretation, the short-range fluctuating order hosts domain walls with quasi-free spins (32, 33). These are called "orphan" spins. Presumably, interaction between these gives the observed power-law dependence with temperature. It should be emphasized that they are not related to impurities, which are structural defects in the system. They are intimately linked to the QSL nature of the magnetic structure. This explains the sample-independent behavior and that one can observe these features in other QSL candidates, as well (32, 33).

Conclusion

The materialization of QSLs continues to be a very challenging field. A deep understanding of this phenomenon needs materials carrying a broad range of microscopic parameters. The EDT-BCO is a material which realizes a QSL state. In this material, the randomly frozen positions of the BCO rotor molecules generate a disorder potential. Even though DFT calculations predict magnetic order within the spin-carrying EDT layers, this disorder potential stymies the magnetic order, leading to a QSL state. This report offers a toolbox for making a broad class of molecular quantum spin-liquid systems with various architectures, where built-in disorder generates QSL behavior.

Materials and Methods

Synthesis. Single crystals of $[EDT\text{-}TTF\text{-}CONH_2]_2^+[BABCO^-]$ (for ESR and transport measurements) and additional significant amounts (ca. 100 mg) of crystalline samples for NMR and μSR experiments were synthesized as described in ref. 27.

The crystal structure, monoclinic unit cell, space group *Pa*, has no inversion symmetry with two independent molecules (different carbon–carbon double-bond lengths) of the *A* and *B* molecules of the dimers (1.33 and 1.40 Å, respectively; Fig. 1*C*) (27).

Unlike in the case of δ-$(EDT\text{-}TTF\text{-}CONMe_2)_2X$ (X = AsF_6, Br) (54), the large size of the Brownian rotor molecules and the hydrogen bonding in between the neighboring $[BABCO^-]$ components (cf. Fig. 1*B*) exclude the low-temperature charge ordering.

Nuclear Magnetic Resonance. Experiments were conducted in polycrystalline samples at a ^{1}H Larmor frequency of 62 MHz down to 5 K. Wide-line ^{1}H spectra were measured using a home-built NMR spectrometer and probe. The probe was designed to reduce spurious proton signals. Samples were loaded into a small glass tube (1.2 to 1.6 mm in diameter) on which the NMR coil was wound. The ^{1}H signals were recorded using the free induction decay following a $\pi/2$ pulse (typically 0.8 to 1.5 μs), and spin-lattice relaxation was measured using the standard saturation recovery sequence. For each T_1 measurement, we recorded signals for 20 values of the relaxation delay between the saturating comb and the measuring pulse.

Electron Spin Resonance. Multifrequency ESR measurements were conducted using a commercial Bruker Elexsys E500 spectrometer in the 4- to 35-GHz frequency range and a home-built high-frequency ESR spectrometer using the induction mode in the 52- to 420-GHz frequency range in the 1.5- to 300-K temperature range. The spectral resolution of ESR is linearly proportional to the frequency, and thus we extended the precision of ESR by about a factor of 40, when compared with the X-band ESR technique. More details about the setup can be found in refs. 55 and 56. The magnetic-field strength at the sample position was calibrated against a KC_{60} standard sample.

$[EDT\text{-}TTF\text{-}CONH_2]_2^+[BABCO^-]$ has a single ESR line corresponding to the spins in the cation plane. Measurements were performed in single crystals of EDT-BCO in the three main *g*-factor orientations and angular-dependent studies were performed at several temperatures to confirm the absence of change of the *g* factors as a function of temperature.

PHYSICS

Muon Spin Rotation. μSR experiments were performed in the ISIS Rutherford Appleton Laboratory and in the Swiss Muon Source. Experimental data were analyzed using the WiMDA program (57) and MuSRFit. Zero- and longitudinal-field data were collected from 19 mK to 300 K at fixed temperatures.

Magnetic Exchange Calculations. Pairwise magnetic exchange interactions between $[\text{EDT-TTF-CONH}_2]^+$ dimers were estimated via relativistic DFT calculations combined with exact diagonalization of a generalized Hubbard Hamiltonian (36) on four molecule clusters. This approach accounts for the internal electronic degrees of freedom within each dimer, which may modify the effective exchange interactions. Hopping integrals, including spin–orbit coupling, were estimated using the local quantum chemistry package ORCA on pairs of molecules at the B3LYP/def2-SV(P) level (58). The two-particle exchange parameters were chosen as previously used for κ-$(\text{ET})_2\text{X}$ materials (36), with the on-site Coulomb repulsion energy $U = 0.55$ eV, the Hund's coupling constant $J_\text{H} = 0.2$ eV, and the intersite Coulomb repulsion energy $V = 0.15$ eV. Exact diagonalization of the resulting Hubbard Hamiltonian, and mapping onto the low-energy subspace, provided a determination of the magnetic exchange parameters, including all anisotropic terms allowed by symmetry.

Data Availability. All the scripts and all the experimental data used to produce the figures within this work are available at Zenodo, https://doi.org/10.5281/zenodo.4130347.

ACKNOWLEDGMENTS. This work was supported by the Swiss National Science Foundation (Grant 200021 144419). Fruitful discussions with András Jánossy, Péter Matus, Stephen M. Winter, Roser Valentí, and Enric Canadell are acknowledged.

1. Y. Shimizu, K. Miyagawa, K. Kanoda, M. Maesato, G. Saito, Spin liquid state in an organic Mott insulator with a triangular lattice. *Phys. Rev. Lett.* **91**, 107001 (2003).
2. T. Itou, A. Oyamada, S. Maegawa, M. Tamura, R. Kato, Quantum spin liquid in the spin-1/2 triangular antiferromagnet $\text{EtMe}_3\text{Sb}[\text{Pd(dmit)}_2]_2$. *Phys. Rev. B* **77**, 104413 (2008).
3. T. Itou, A. Oyamada, S. Maegawa, R. Kato, Instability of a quantum spin liquid in an organic triangular-lattice antiferromagnet. *Nat. Phys.* **6**, 673–676 (2010).
4. T. Isono *et al.*, Gapless quantum spin liquid in an organic spin-1/2 triangular-lattice κ-$\text{H}_3(\text{Cat-EDT-TTF})_2$. *Phys. Rev. Lett.* **112**, 177201 (2014)
5. T. H. Han *et al.*, Fractionalized excitations in the spin-liquid state of a kagome-lattice antiferromagnet. *Nature* **492**, 406–410 (2012).
6. L. Clark *et al.*, Gapless spin liquid ground state in the S=1/2 vanadium oxyfluoride kagome antiferromagnet $[\text{NH}_4]_2[\text{C}_7\text{H}_{14}\text{N}][\text{V}_7\text{O}_6\text{F}_{18}]$. *Phys. Rev. Lett.* **110**, 207208 (2013).
7. P. W. Anderson, Resonating valence bonds: A new kind of insulator? *Mater. Res. Bull.* **8**, 153–160 (1973).
8. C. Lacroix, P. Mendels, F. Mila, Eds., *Introduction to Frustrated Magnetism* (Springer Berlin Heidelberg, 2011).
9. L. Balents, Spin liquids in frustrated magnets. *Nature* **464**, 199–208 (2010).
10. X. G. Wen, Quantum orders and symmetric spin liquids. *Phys. Rev. B* **65**, 165113 (2002).
11. P. Fazekas, P. W. Anderson, On the ground state properties of the anisotropic triangular antiferromagnet. *Philos. Mag. A* **30**, 423–440 (1974).
12. Y. Shimizu *et al.*, Pressure-tuned exchange coupling of a quantum spin liquid in the molecular triangular lattice κ-$(\text{ET})_2\text{Ag}_2(\text{CN})_3$. *Phys. Rev. Lett.* **117**, 107203 (2016).
13. Y. Yoshida *et al.*, Spin-disordered quantum phases in a quasi-one-dimensional triangular lattice. *Nat. Phys.* **11**, 679–683 (2015).
14. B. J. Powell, R. H. McKenzie, Quantum frustration in organic Mott insulators: From spin liquids to unconventional superconductors. *Rep. Prog. Phys.* **74**, 056501 (2011).
15. F. L. Pratt *et al.*, Magnetic and non-magnetic phases of a quantum spin liquid. *Nature* **471**, 612–616 (2011).
16. L. Savary, L. Balents, Disorder-induced quantum spin liquid in spin ice pyrochlores. *Phys. Rev. Lett.* **118**, 087203 (2017).
17. B. J. Powell, E. P. Kenny, J. Merino, Dynamical reduction of the dimensionality of exchange interactions and the "spin-liquid" phase of κ-$[\text{BEDT-TTF}]_2\text{X}$. *Phys. Rev. Lett.* **119**, 087204 (2017).
18. L. Capriotti, A. E. Trumper, S. Sorella, Long-range Néel order in the triangular Heisenberg model. *Phys. Rev. Lett.* **82**, 3899–3902 (1999).
19. W. LiMing, G. Misguich, P. Sindzingre, C. Lhuillier, From Néel long-range order to spin liquids in the multiple-spin exchange model. *Phys. Rev. B* **62**, 6372–6377 (2000).
20. B. Bernu, P. Lecheminant, C. Lhuillier, L. Pierre, Exact spectra, spin susceptibilities, and order parameter of the quantum Heisenberg antiferromagnet on the triangular lattice. *Phys. Rev. B* **50**, 10048–10062 (1994).
21. O. I. Motrunich, Variational study of triangular lattice spin-1/2 model with ring exchanges and spin liquid state in κ-$(\text{ET})_2\text{Cu}_2(\text{CN})_3$. *Phys. Rev. B* **72**, 045105 (2005).
22. Y. Iqbal, W. J. Hu, R. Thomale, D. Poilblanc, F. Becca, Spin liquid nature in the Heisenberg J_1-J_2 triangular antiferromagnet. *Phys. Rev. B* **93**, 144411 (2016).
23. K. Watanabe, H. Kawamura, H. Nakano, T. Sakai, Quantum spin-liquid behavior in the spin-1/2 random Heisenberg antiferromagnet on the triangular lattice. *J. Phys. Soc. Japan* **83**, 034714 (2014).
24. T. Shimokawa, K. Watanabe, H. Kawamura, Static and dynamical spin correlations of the S=1/2 random-bond antiferromagnetic Heisenberg model on the triangular and kagome lattices. *Phys. Rev. B* **92**, 134407 (2015).
25. H. Q. Wu, S. S. Gong, D. N. Sheng, Randomness-induced spin-liquid-like phase in the spin-$\frac{1}{2}$ $J_1 - J_2$ triangular Heisenberg model. *Phys. Rev. B* **99**, 085141 (2019).
26. T. Furukawa *et al.*, Quantum spin liquid emerging from antiferromagnetic order by introducing disorder. *Phys. Rev. Lett.* **115**, 077001 (2015).
27. C. Lemouchi *et al.*, Design and evaluation of a crystalline hybrid of molecular conductors and molecular rotors. *J. Am. Chem. Soc.* **134**, 7880–7891 (2012).
28. O. A. Starykh, L. Balents, Ordering in spatially anisotropic triangular antiferromagnets. *Phys. Rev. Lett.* **98**, 077205 (2007).
29. T. Pardini, R. Singh, Magnetic order in coupled spin-half and spin-one Heisenberg chains in an anisotropic triangular-lattice geometry. *Phys. Rev. B* **77**, 214433 (2008).
30. C. S. Vogelsberg *et al.*, Ultrafast rotation in an amphidynamic crystalline metal organic framework. *Proc. Natl. Acad. Sci. U.S.A.* **114**, 13613–13618 (2017).
31. C. Lemouchi *et al.*, Crystalline arrays of pairs of molecular rotors: Correlated motion, rotational barriers, and space-inversion symmetry breaking due to conformational mutations. *J. Am. Chem. Soc.* **135**, 9366–9376 (2013).
32. I. Kimchi, A. Nahum, T. Senthil, Valence bonds in random quantum magnets: Theory and application to YbMgGaO_4. *Phys. Rev. X* **8**, 031028 (2018).
33. K. Riedl, R. Valentí, S. M. Winter, Critical spin liquid versus valence-bond glass in a triangular-lattice organic antiferromagnet. *Nat. Commun.* **10**, 2561 (2019).
34. T. Nakamura *et al.*, ESR properties of κ-type organic superconductors based on BEDT-TTF. *J. Phys. Soc. Japan* **63**, 4110–4125 (1994).
35. M. Dumm *et al.*, Comprehensive ESR study of the antiferromagnetic ground states in the one-dimensional spin systems $(\text{TMTSF})_2\text{PF}_6$,$(\text{TMTSF})_2\text{AsF}_6$, and $(\text{TMTTF})_2\text{Br}$. *Phys. Rev. B* **62**, 6512 (2000).
36. S. M. Winter, K. Riedl, R. Valentí, Importance of spin-orbit coupling in layered organic salts. *Phys. Rev. B* **95**, 060404 (2017).
37. Á. Antal, T. Fehér, Á. Jánossy, E. Tátrai-Szekeres, F. Fülöp, Spin diffusion and magnetic eigenoscillations confined to single molecular layers in the organic conductors κ-$(\text{BEDT-TTF})_2$ $\text{Cu}[\text{N(CN)}_2]\text{X}$ (X= Cl, Br). *Phys. Rev. Lett.* **102**, 086404 (2009).
38. Á. Antal, T. Fehér, B. Náfrádi, L. Forró, T. Jánossy, Two-dimensional magnetism in κ-$(\text{BEDT-TTF})_2\text{Cu}[\text{N(CN)}_2]\text{Cl}$, a spin-1/2 Heisenberg antiferromagnet with Dzyaloshinskii–Moriya interaction. *J. Phys. Soc. Japan* **84**, 124704 (2015).
39. P. Anderson, P. Weiss, Exchange narrowing in paramagnetic resonance. *Rev. Mod. Phys.* **25**, 269 (1953).
40. P. Anderson, A mathematical model for the narrowing of spectral lines by exchange or motion. *J. Phys. Soc. Japan* **9**, 316–339 (1954).
41. J. M. Abendroth, O. S. Bushuyev, P. S. Weiss, Controlling motion at the nanoscale: Rise of the molecular machines. *ACS Nano* **9**, 7746–7768 (2015)
42. N. Bloembergen, E. M. Purcell, R. V. Pound, Relaxation effects in nuclear magnetic resonance absorption. *Phys. Rev. E* **73**, 679–712 (1948).
43. Y. Uemura, μSR relaxation functions in magnetic materials. *Muon Sci. Muons Phys. Chem. Mater.***51**, 85–114 (1999).
44. B. Fåk *et al.*, Kapellasite: A kagome quantum spin liquid with competing interactions. *Phys. Rev. Lett.* **109**, 037208 (2012).
45. E. Kermarrec *et al.*, Spin-liquid ground state in the frustrated kagome antiferromagnet $\text{MgCu}_3(\text{OH})_6\text{Cl}_2$. *Phys. Rev. B* **84**, 100401 (2011).
46. F. L. Pratt, S. J. Blundell, T. Lancaster, C. Baines, S. Takagi, Low-temperature spin diffusion in a highly ideal S=1/2 Heisenberg antiferromagnetic chain studied by muon spin relaxation. *Phys. Rev. Lett.* **96**, 247203 (2006).
47. F. Xiao *et al.*, Spin diffusion in the low-dimensional molecular quantum Heisenberg antiferromagnet $\text{Cu(pyz)(NO}_3)_2$ detected with implanted muons. *Phys. Rev. B* **91**, 144417(2015).
48. M. Žnidarič, Spin transport in a one-dimensional anisotropic Heisenberg model. *Phys. Rev. Lett.* **106**, 220601 (2011).
49. A. T. Ogielski, Dynamics of three-dimensional Ising spin glasses in thermal equilibrium. *Phys. Rev. B* **32**, 7384–7398 (1985).
50. A. Keren, G. Bazalitsky, I. Campbell, J. S. Lord, Probing exotic spin correlations by muon spin depolarization measurements with applications to spin glass dynamics. *Phys. Rev. B* **64**, 054403 (2001).
51. T. McMullen, E. Zaremba, Positive-muon spin depolarization in solids. *Phys. Rev. B* **18**, 3026–3040 (1978).
52. F. Iglói, C. Monthus, Strong disorder RG approach of random systems. *Phys. Rep.* **412**, 277–431 (2005).
53. Y. Li *et al.*, Muon spin relaxation evidence for the U(1) quantum spin-liquid ground state in the triangular antiferromagnet YbMgGaO_4. *Phys. Rev. Lett.* **117**, 097201 (2016).
54. L. Zorina *et al.*, Charge ordering, symmetry and electronic structure issues and Wigner crystal structure of the quarter-filled band Mott insulators and high pressure metals δ-$(\text{EDT-TTF-CONMe}_2)_2X$, X=Br and AsF_6. *J. Mater. Chem.* **19**, 6980–6994 (2009).
55. B. Náfrádi, R. Gaál, A. Sienkiewicz, T. Fehér, L. Forró, Continuous-wave far-infrared ESR spectrometer for high-pressure measurements. *J. Magn. Reson.* **195**, 206–210 (2008).
56. B. Náfrádi, R. Gaál, T. Fehér, L. Forró, Microwave frequency modulation in continuous-wave far-infrared ESR utilizing a quasi-optical reflection bridge. *J. Magn. Reson.* **192**, 265–268 (2008).
57. F. L. Pratt, Wimda: A muon data analysis program for the Windows PC. *Phys. B Condens. Matter* **289–290**, 710–714 (2000).
58. F. Neese, The ORCA program system. *Wiley Interdiscip. Rev. Comput. Mol. Sci.* **2**, 73–78 (2012).